PROCEEDINGS A

royalsocietypublishing.org/journal/rspa

Research



Cite this article: Schimming CD, Vinals J. 2024 A tensor density measure of topological charge in three-dimensional nematic phases. *Proc. R.*

Soc. A 480: 20230564.

https://doi.org/10.1098/rspa.2023.0564

Received: 4 August 2023 Accepted: 25 March 2024

Subject Areas:

materials science

Keywords:

nematic liquid crystals, topological defects, disclinations, Skyrmions

Author for correspondence:

Cody D. Schimming e-mail: cschim@lanl.gov

A tensor density measure of topological charge in three-dimensional nematic phases

Cody D. Schimming¹ and Jorge Vinals²

¹Theoretical Division and Center for Nonlinear Studies, Los Alamos National Laboratory, Los Alamos, NM 87545, USA,

²School of Physics and Astronomy, University of Minnesota, Minneapolis, MN 55455, USA

© CDS, 0000-0003-2143-6738

A path-independent measure in order parameter space is introduced such that, when integrated along any closed contour in a three-dimensional nematic phase, it yields the topological charge of any line defects encircled by the contour. A related measure, when integrated over either closed or open surfaces, reduces to known results for the charge associated with point defects (hedgehogs) or Skyrmions. We further define a tensor density, the disclination density tensor D, from which the location of a disclination line can be determined. This tensor density has a dyadic decomposition near the line into its tangent and its rotation vector, allowing a convenient determination of both. The tensor D may be non-zero in special configurations in which there are no defects (double-splay or double-twist configurations), and its behaviour there is provided. The special cases of Skyrmions and hedgehog defects are also examined, including the computation of their topological charge from D.

1. Introduction

The study of line defects in three-dimensional nematic phases, known as disclinations, has gained considerable interest recently following advances in both experimental diagnostics and computational methods [1–6]. Disclinations and their motion have found applications in microfluidics, colloidal self-assembly, surface actuation, optical control and active and biological matter [7–16]. Recent theoretical research has also advanced our understanding of disclinations, including

measures of their topology and geometry, as well as analytical results for disclination kinematics [17–21].

The well-established definition of the topological charge m of a disclination in two-dimensional nematics can be expressed as a function of the director angle ϕ , the director $\hat{\mathbf{n}}$ or the tensor order parameter \mathbf{Q} [22], as

$$m = \frac{1}{2\pi} \oint_C \partial_k \phi \, d\ell_k, \tag{1.1}$$

$$= \frac{1}{2\pi} \oint_{C} \varepsilon_{\mu\nu} \hat{n}_{\mu} \partial_{k} \hat{n}_{\nu} d\ell_{k}, \tag{1.2}$$

$$=\frac{1}{2\pi S_N^2} \oint_{C^*} \varepsilon_{\mu\nu} Q_{\mu\alpha} \partial_k Q_{\nu\alpha} d\ell_k, \tag{1.3}$$

where repeated indices are summed over, and C and C^* are closed curves encircling the defect, but the latter is restricted to a path far from the core in which the scalar order parameter $S = S_N$ is constant. $\epsilon_{\mu\nu}$ is the Levi–Civita tensor in two dimensions. Stokes' theorem may be applied and the line integrals transformed to surface integrals over surfaces bounded by curves C or C^* . The integrands of these surface integrals may then be regarded as locally defined 'densities', carrying information about the topological charge. For the case of the singular quantities ϕ and $\hat{\mathbf{n}}$, these densities are Dirac delta functions located at cores of defects. For the case of equation (1.3), this density is a diffuse scalar field with maxima or minima located at defect cores.

Generalizing equations (1.1)-(1.3) to three-dimensional disclination lines has not been possible due to several added complications. First, the topology of the ground-state manifold is different between two- and three-dimensional nematics. The ground-state manifold in three dimensions is the two-dimensional real projective space \mathbb{RP}^2 , which is not isomorphic to the unit sphere, and is non-orientable. This space is equivalent to a hemisphere in which all points on the equator are identified with their polar opposites [23]. This results in all line disclinations having a topological charge of +1/2, and any two disclinations that come into contact will annihilate [23]. This is in contrast with two dimensions. There, the ground-state manifold is \mathbb{RP}^1 , which is isomorphic to the unit circle S^1 . Disclinations in two dimensions can have positive and negative charges, and they combine according to well-established rules. An invariant measure of charge can be readily defined in two dimensions from closed paths on the circle, equations (1.1)-(1.3). In three-dimensional space, two angles are needed to describe the director orientation. With this added dimensionality, equations (1.1)-(1.3) do not have a direct generalization as a continuum of circuits can be constructed encircling a disclination that leads to a different length in order parameter space. An extension of these expressions to paths on \mathbb{RP}^2 has not yet been given, and it is the subject of our work below.

Downloaded from https://royalsocietypublishing.org/ on 16 September 2024

Second, the geometric structure of disclination lines in three dimensions is quite complex as they can be of wedge, twist or mixed type [13,22]. Disclination interactions and motion are governed not just by their topological charge but by their geometrical structure as well. It is well established that the geometry of the disclination line can be characterized by a single vector, the rotation vector $\hat{\boldsymbol{\Omega}}$: the director and its distortion in the vicinity of the disclination lie on the plane defined by $\hat{\boldsymbol{\Omega}}$. Note that $\hat{\boldsymbol{\Omega}}$ itself may change along the disclination line.

Finally, three-dimensional systems allow biaxiality, and they are commonly described by the tensor order parameter \mathbf{Q} . Although \mathbf{Q} relieves some of the representational issues that the director has, it is a more complicated object with its distinct order parameter space and topological classes. In the vicinity of a disclination core, nematic configurations become biaxial in three dimensions, and \mathbf{Q} does not go to zero at the core [1,24]. Results involving \mathbf{Q} are presented below, but restricted to paths in real space in which the order parameter remains

uniaxial. This is the case for distances away from the defect core larger than the coherence length of \mathbf{Q} .

In recent work [20], we introduced a tensor density \mathbf{D} , function of either the director $\hat{\mathbf{n}}$ or the tensor order parameter \mathbf{Q} , which is non-zero near disclination cores, but also near some non-singular textures. The formula yielding \mathbf{D} in Ref. [20] is based on a path integral for the arclength of the corresponding curve in order parameter space. However, the integral given is not a topological invariant, and therefore does not generalize equations (1.1)–(1.3). Despite that the path integral in Ref. [20] is not an invariant, the measure \mathbf{D} is still useful in locating and characterizing disclination lines. It can also be related to the Jacobian of the transformation between real space and order parameter space, and leads to an exact kinematic law relating the velocity of a disclination line and the time derivative of the order parameter \mathbf{Q} [21]. Therefore, a clearer connection between \mathbf{D} and an invariant measure of the charge is desirable both mathematically, and for practical experimental and computational applications. Such a precise connection is the subject matter of the present paper. Furthermore, since the density \mathbf{D} may be non-zero for nematic textures that do not contain disclination lines, we also investigate below the properties of \mathbf{D} for such textures.

In this work, an invariant measure is introduced such that, when integrated along any closed contour in a three-dimensional nematic configuration, it yields the topological charge of any line defects encircled by the contour. Such an invariant measure differs from previous constructions in that either the director or **Q**-tensor may be used in its computation. We further show that the tensor density **D** already introduced in Ref. [20] may be derived from this invariant measure, and discuss under what conditions **D** may be non-zero away from disclination lines, but still yield an invariant integral. Our results generalize equations (1.1)–(1.3) to three dimensions, and provide an expression to compute the topological charge within a region of a three-dimensional nematic. We note that the measure presented here is different from the one used in Ref. [20], since the integral computed there is not a topological invariant.

Additionally, we explore cases in which **D** is non-zero in configurations that do not contain disclinations. For example, double-splay and double-twist nematic distortions generally give non-zero **D**. We also extend our analysis to Skyrmions and point defects, both of which have had a long history of research and are of current interest for applications involving the design of unique meta-materials, colloidal assembly and electroosmotic control of biomaterials [25–31]. We show that **D** may be used to compute their topological charge, and to identify them, even as the structure of **D** differs substantially depending on the topological object under consideration.

2. An invariant measure of disclination charge

We introduce a mathematical construction that generalizes equations (1.1)–(1.3) to three dimensions, where the topological charge of a disclination line is always +1/2. We thus seek to construct a path integral in order parameter space that equals either 0 or π , modulo 2π , for any corresponding closed circuit in real space. To accomplish this, we construct a path integral on the unit sphere that always gives the geodesic distance between the endpoints of the path, and hence is independent of the path chosen. For closed curves, this calculation results in either 0 or π modulo 2π since closed curves in real space map onto either closed curves or curves with endpoints at opposite ends of the equator in order parameter space.

Given a path in real space, we may map the director along the curve to points on the unit hemisphere, $\hat{\mathbf{n}}(s)$, where s is an arclength parameterization. The quantity $\hat{\mathbf{n}}(s) \times d\hat{\mathbf{n}}(s)$ gives the rotation of the director about the axis projected onto it [32]. Hence, the corresponding element of length of a curve in order parameter space is $ds^2 = |\hat{\mathbf{n}}(s) \times d\hat{\mathbf{n}}(s)|^2$. However, we do not seek to

¹We thank Jonathan Selinger for pointing this fact out to us, and for providing the counterexample involving double-splay and double-twist.

compute the length of the given curve, but rather the geodesic distance between its endpoints. We first fix a reference point along the curve defined as $\hat{\mathbf{n}}(0) = \hat{\mathbf{n}}^*$. Then, at each point along the curve, we define the unit vector

$$\hat{\mathbf{M}}(s) = \frac{\hat{\mathbf{n}}(s) \times \hat{\mathbf{T}}_{GC}(s)}{|\hat{\mathbf{n}}(s) \times \hat{\mathbf{T}}_{GC}(s)|},$$
(2.1)

where $\hat{\mathbf{T}}_{GC}(s)$ is the tangent vector to the great circle defined by the current point $\hat{\mathbf{n}}(s)$ and the fixed point $\hat{\mathbf{n}}^*$. Projecting this into $\hat{\mathbf{n}} \times d\hat{\mathbf{n}}$ gives

$$\hat{\mathbf{M}}(s) \cdot \left[\hat{\mathbf{n}}(s) \times d\hat{\mathbf{n}}(s) \right] = \frac{\hat{\mathbf{T}}_{GC}(s) \cdot d\hat{\mathbf{n}}(s)}{|\hat{\mathbf{n}}(s) \times \hat{\mathbf{T}}_{GC}(s)|} = d\varsigma(s), \tag{2.2}$$

where we have introduced the notation $\varsigma(s)$ to indicate the geodesic distance between $\hat{\mathbf{n}}^*$ and $\hat{\mathbf{n}}(s)$.

To explicitly compute $\int d\varsigma$, we define the unit vector

$$\hat{\mathbf{V}}(s) = a(s)\hat{\mathbf{n}}^* + b(s)\hat{\mathbf{n}}(s), \tag{2.3}$$

where a(s) and b(s) are determined by requiring that $\hat{\mathbf{V}}(s) \cdot \hat{\mathbf{n}}^* = 0$. Given, $\hat{\mathbf{n}}^*$ and $\hat{\mathbf{n}}(s)$, this can always be achieved via the Gram–Schmidt procedure. Then, the curve

$$\hat{\mathbf{W}}(t,s) = \cos t \hat{\mathbf{n}}^* + \sin t \hat{\mathbf{V}}(s), \tag{2.4}$$

parameterizes the great circle on the unit sphere passing through both $\hat{\mathbf{n}}^*$ and $\hat{\mathbf{n}}(s)$ for any s. In particular, we have that $\hat{\mathbf{W}}(t^*(s), s) = \hat{\mathbf{n}}(s)$ for $t^*(s) = -\arctan[1/a(s)]$. With this parameterization of the great circle, equation (2.2) may be written as

$$d\varsigma(s) = \frac{d\hat{\mathbf{w}}/dt \cdot d\hat{\mathbf{n}}/ds}{|\hat{\mathbf{n}} \times d\hat{\mathbf{w}}/dt|} \bigg|_{t = t^*(s)} ds.$$
 (2.5)

Substituting the definition (2.4), and integrating over the curve, one has

$$\int_{C} d\varsigma(s) = \int_{C} \frac{\hat{\mathbf{n}}(0) \cdot d\hat{\mathbf{n}}/ds}{|\hat{\mathbf{n}}(0) \times \hat{\mathbf{n}}(s)|} ds = \int_{C} \frac{\hat{\mathbf{n}}^{*} \cdot d\hat{\mathbf{n}}}{|\hat{\mathbf{n}}^{*} \times \hat{\mathbf{n}}|}.$$
 (2.6)

Note that

$$\nabla_{\hat{\mathbf{n}}} \times \frac{\hat{\mathbf{n}}^*}{|\hat{\mathbf{n}}^* \times \hat{\mathbf{n}}|} = 0, \tag{2.7}$$

where $\nabla_{\hat{\mathbf{n}}}$ denotes a derivative in order parameter space, a result that can be proved by direct substitution in spherical coordinates. Therefore, $d\varsigma$ is an exact differential on the hemisphere.

If the curve C in equation (2.6) does not cross the equator of the unit sphere, the integral is zero because $d\varsigma$ is an exact differential and the curve starts and ends at the same point. On the other hand, if the curve does cross the equator then, since the integral is independent of the path, it will be equal to π as this is the result for the shortest path joining the two points. In general, π must be added to the contour integral for each time the equator is crossed, because this is the length of the arc of a great circle connecting the two identified points on the equator. A subtle point here is that if the equator is passed an even number of times the measured configuration in three dimensions is topologically equivalent to a configuration with no disclinations. This is not represented by our measure since we are representing the ground state manifold (\mathbb{RP}^2) with vectors, and so we must impose that the resulting calculation is valid modulo 2π

$$\oint_C d\varsigma(s) \in \{0, \pi\} \text{ modulo } 2\pi. \tag{2.8}$$

This is our central result concerning a path invariant measure on \mathbb{RP}^2 . This result (which originates from equations (2.6) and (2.7)) differs from eqn (3) in Ref. [20].

The construction is graphically illustrated in figure 1 including the cases $\oint_C d\varsigma(s)$ equal 0 or π depending on whether the curve does or does not pass through the equator. Note that the curves in both figure 1b,c are considered closed curves in the nematic order parameter space. Appendix A shows the analogous construction of a path integral in Euclidean space, such that the integral gives the distance between the two endpoints of any path connecting them. This is provided to give some context and clarity to the above mathematical construction and proof.

We may summarize our result for the charge of a disclination in the following way in terms of the measuring circuit in real space

$$\pi m = \oint_{C} \hat{M}_{\gamma} \varepsilon_{\gamma\mu\nu} \hat{n}_{\mu} \partial_{k} \hat{n}_{\nu} d\ell_{k} \text{ modulo } 2\pi,$$

$$\pi m = \frac{1}{S_{N}^{2}} \oint_{C^{*}} \hat{M}_{\gamma} \varepsilon_{\gamma\mu\nu} Q_{\mu\alpha} \partial_{k} Q_{\nu\alpha} d\ell_{k} \text{ modulo } 2\pi,$$
(2.9)

where we have used the identity $S_N^2(\hat{\mathbf{n}} \times \nabla \hat{\mathbf{n}}) = \mathbf{Q} \times \nabla \mathbf{Q}$ for a uniaxial nematic with constant $S = S_N$. These results are independent of the circuit chosen.

It is interesting to note that as a measuring curve C encircling a disclination line is taken to be smaller and smaller, the resulting curve on the ground-state manifold itself approaches a great circle. In this limit, the vector $\hat{\mathbf{M}}$ becomes identical to the rotation vector $\hat{\boldsymbol{\Omega}}$, which describes the plane in which the director lies close to the disclination line in its normal plane.

Finally, we give an explicit example of computing equation (2.6). Consider a straight disclination line such that the rotation vector $\hat{\Omega}$ changes along the line. Since the line is straight, the director in each normal plane is given by:

$$\hat{\mathbf{n}} = \hat{\mathbf{n}}_0 \cos \frac{\varphi}{2} + \hat{\mathbf{n}}_1 \sin \frac{\varphi}{2},\tag{2.10}$$

where $\{\hat{\mathbf{n}}_0, \hat{\mathbf{n}}_1, \hat{\mathbf{\Omega}}\}\$ is an orthonormal triad, and φ is the azimuthal angle in the normal plane to the disclination. Let the disclination lie along the z-axis and let the explicit form of $\hat{\mathbf{\Omega}}(z) = \hat{\mathbf{y}}\sin z + \hat{\mathbf{z}}\cos z$ with $\hat{\mathbf{n}}_0 = \hat{\mathbf{x}}$ so that $\hat{\mathbf{n}}_1(z) = -\hat{\mathbf{z}}\sin z + \hat{\mathbf{y}}\cos z$. Now, consider two curves that encircle the disclination:

$$\begin{split} \gamma_1(t) &= (\cos t, \sin t, 0), \quad 0 \leq t \leq 2\pi \\ \gamma_2(t) &= \begin{cases} (\cos t, \sin t, t), & 0 \leq t \leq \pi \\ (\cos t, \sin t, 2\pi - t), & \pi \leq 2\pi \end{cases}. \end{split}$$

 γ_1 is a circle in the normal plane of the disclination, while γ_2 is a piecewise differentiable curve that tilts out of the normal plane. The director along γ_1 is given by $\hat{\mathbf{n}}(t) = \hat{\mathbf{x}}\cos(t/2) + \hat{\mathbf{y}}\sin(t/2)$ and we choose $\hat{\mathbf{n}}^* = \hat{\mathbf{n}}(0) = \hat{\mathbf{x}}$. Along this curve, the integral equation (2.6) is given by:

$$\int_0^{2\pi} \frac{\mathbf{\hat{n}}^* \cdot d\mathbf{\hat{n}}/dt}{|\mathbf{\hat{n}}^* \times \mathbf{\hat{n}}(t)|} dt = -\frac{1}{2} \int_0^{2\pi} \frac{\sin(t/2)}{\sin(t/2)} dt = -\pi,$$

which is π modulo 2π as expected. The director along the second curve is given by $\hat{\mathbf{n}}(t) = \hat{\mathbf{x}}\cos(t/2) + [\hat{\mathbf{y}}\cos t \mp \hat{\mathbf{z}}\sin t]\sin(t/2)$, where the minus applies from $0 \le t \le \pi$ and the plus applies from π §lt; $t \le 2\pi$. A similar calculation to the first curve yields

$$\int_0^\pi \frac{\hat{\mathbf{n}}^* \cdot d\hat{\mathbf{n}}/dt}{|\hat{\mathbf{n}}^* \times \hat{\mathbf{n}}(t)|} \, dt + \int_\pi^{2\pi} \frac{\hat{\mathbf{n}}^* \cdot d\hat{\mathbf{n}}/dt}{|\hat{\mathbf{n}}^* \times \hat{\mathbf{n}}(t)|} \, dt = -\frac{1}{2} \int_0^\pi \frac{\sin(t/2)}{\sin(t/2)} \, dt - \frac{1}{2} \int_\pi^{2\pi} \frac{\sin(t/2)}{\sin(t/2)} \, dt = -\pi,$$

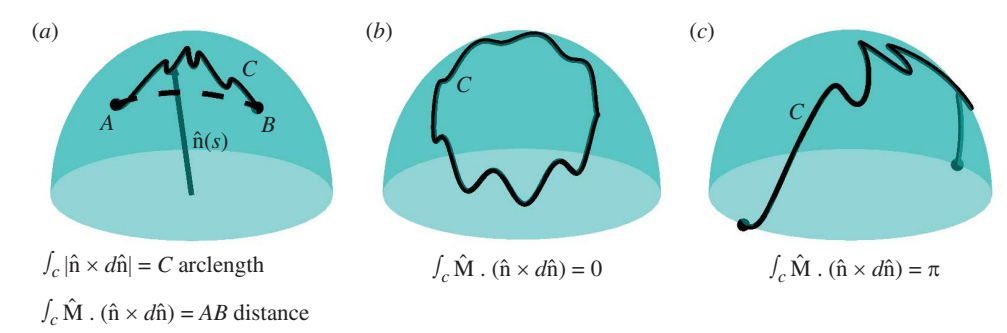


Figure 1. Illustration of curves in nematic order parameter space and corresponding path integrals. (*a*) Curve *C* connecting two points *A* and $B \not\subset |\hat{\mathbf{n}} \times d\hat{\mathbf{n}}|$. $\int |\hat{\mathbf{n}} \times d\hat{\mathbf{n}}|$ gives the arclength of contour *C*, while $\int_C \hat{\mathbf{M}} \cdot (\hat{\mathbf{n}} \times d\hat{\mathbf{n}})$ with $\hat{\mathbf{M}}$ given by equation (2.1), gives the geodesic distance between *A* and *B*. The dashed line shows the segment of great circle defined by *A* and *B*, the length of which gives the shortest distance between the two. (*b*) A closed curve *C* which does not pass through the equator. In this case, $\int_C \hat{\mathbf{M}} \cdot (\hat{\mathbf{n}} \times d\hat{\mathbf{n}}) = 0$. (*c*) A closed curve *C* which passes through the equator. In this case, $\int_C \hat{\mathbf{M}} \cdot (\hat{\mathbf{n}} \times d\hat{\mathbf{n}}) = \pi$.

where the integral is split along the two differentiable pieces of the curve.

The above example illustrates two useful features of the invariant integral. First, particularly in non-equilibrium settings such as flowing or active nematics, the rotation vector may vary along the curve [13,14]. In this case, any curve that encircles the disclination will still measure the correct topological charge of the disclination. Second, the curve chosen need only be piecewise differentiable, allowing potentially more convenient choices of measuring curves, particularly if the integrals must be performed numerically.

(a) The disclination density tensor **D**

Equation (2.9) may be used to locate disclination lines in a configuration. In practice, however, it is complicated to compute \mathbf{M} for various circuits C. Additionally, many curves must be constructed to completely locate the line. Therefore, just as is done in two dimensions, we construct a density by applying Stokes' theorem to equation (2.9). The curl of the integrand of equation (2.9) is given by:

$$\varepsilon_{ik\ell}\partial_k \left(\hat{M}_{\gamma} \varepsilon_{\gamma\mu\nu} \hat{n}_{\mu} \partial_{\ell} \hat{n}_{\nu} \right) = \varepsilon_{ik\ell} \varepsilon_{\gamma\mu\nu} \left[\partial_k \hat{M}_{\gamma} \hat{n}_{\mu} \partial_{\ell} \hat{n}_{\nu} + \hat{M}_{\gamma} \partial_k \hat{n}_{\mu} \partial_{\ell} \hat{n}_{\nu} + \hat{M}_{\gamma} \hat{n}_{\mu} \partial_k \partial_{\ell} \hat{n}_{\nu} \right], \tag{2.11}$$

$$\varepsilon_{ik\ell}\partial_k \left(\hat{M}_{\gamma} \varepsilon_{\gamma\mu\nu} Q_{\mu\alpha} \partial_{\ell} Q_{\nu\alpha} \right) = \varepsilon_{ik\ell} \varepsilon_{\gamma\mu\nu} \left[\partial_k \hat{M}_{\gamma} Q_{\mu\alpha} \partial_{\ell} Q_{\nu\alpha} + \hat{M}_{\gamma} \partial_k Q_{\mu\alpha} \partial_{\ell} Q_{\nu\alpha} + \hat{M}_{\gamma} Q_{\mu\alpha} \partial_k \partial_{\ell} Q_{\nu\alpha} \right], \tag{2.12}$$

where the derivative of $\hat{\mathbf{M}}$ may be computed by extending its definition to a family of curves that cover the surface of integration. In general, there are three terms that must be integrated over the Stokes surface when computing the charge. If we consider the integrand near a disclination line, however, the expression simplifies significantly.

Near a disclination line, $\hat{\mathbf{M}} \to \hat{\mathbf{\Omega}}$ and the director is given by equation (2.10). Direct substitution of equation (2.10) into equation (2.11) gives $\varepsilon_{\gamma\mu\nu}\hat{n}_{\mu}\partial_{\ell}\hat{n}_{\nu} = (1/2)\hat{\Omega}_{\gamma}\partial_{\ell}\varphi$, and so the first term on the right-hand side of equation (2.11) goes to zero, since $\hat{\Omega}_{\gamma}\partial_{k}\hat{\Omega}_{\gamma} = 0$, while the second term also goes to zero, since $\varepsilon_{ik\ell}\varepsilon_{\gamma\mu\nu}\partial_{k}\hat{n}_{\mu}\partial_{\ell}\hat{n}_{\nu} = 0$ for $\hat{\mathbf{n}}$ given by equation (2.10). This leaves the third term as the only non-zero term for disclinations which gives a delta function due to the

singular nature of the director at the core of the disclination. We note that there are nematic configurations in which the term $\varepsilon_{ikl}\varepsilon_{\mu\nu}\partial_k\hat{n}_\mu\partial_\ell\hat{n}_\nu$ is non-zero. We explore a few cases in §4.

On the other hand, if the \mathbf{Q} tensor representation is used and equation (2.12) applies, a linear core approximation may be used for \mathbf{Q} near the core [19,20]:

$$\mathbf{Q} \approx S_N \left[\frac{1}{6} \mathbf{I} - \frac{1}{2} \mathbf{\hat{\Omega}} \otimes \mathbf{\hat{\Omega}} + \frac{\mathbf{\hat{\nu}}_0 \cdot \mathbf{r}}{2a} (\mathbf{\hat{n}}_0 \otimes \mathbf{\hat{n}}_0 - \mathbf{\hat{n}}_1 \otimes \mathbf{\hat{n}}_1) + \frac{\mathbf{\hat{\nu}}_1 \cdot \mathbf{r}}{2a} (\mathbf{\hat{n}}_0 \otimes \mathbf{\hat{n}}_1 + \mathbf{\hat{n}}_1 \otimes \mathbf{\hat{n}}_0) \right], \tag{2.13}$$

where $\{\hat{\boldsymbol{\nu}}_0, \hat{\boldsymbol{\nu}}_1, \hat{\mathbf{T}}\}$ are an orthonormal triad describing the orientation of the disclination line, and a is the radius of the disclination core. Substituting equation (2.13) into equation (2.12) gives $\varepsilon_{\nu\mu\nu}Q_{\mu\alpha}\partial_{\ell}Q_{\nu\alpha} = S_N^2\hat{\Omega}_{\nu}A_{\ell}$, where

$$\mathbf{A} = \frac{\hat{\mathbf{v}}_0 \cdot \mathbf{r}}{2a^2} \hat{\mathbf{v}}_1 - \frac{\hat{\mathbf{v}}_1 \cdot \mathbf{r}}{2a^2} \hat{\mathbf{v}}_0.$$

Thus, the first term on the left-hand side of equation (2.12) is zero when $\hat{\mathbf{M}} \to \hat{\mathbf{\Omega}}$ for the same reason as above. Furthermore, the third term in equation (2.12) is always zero, regardless of the nematic configuration, since \mathbf{Q} is a non-singular quantity. This leaves the second term on the left-hand side of equation (2.12) as the only non-zero term.

The simplification of equations (2.11) and (2.12) near a disclination core leads to the following definitions:

$$\mathbf{\hat{M}} \cdot \mathbf{D}^{(\hat{\mathbf{n}})} := \hat{M}_{\gamma} \varepsilon_{ik\ell} \partial_k \left(\varepsilon_{\gamma\mu\nu} \hat{n}_{\mu} \partial_{\ell} \hat{n}_{\nu} \right), \tag{2.14}$$

$$\hat{\mathbf{M}} \cdot \mathbf{D}^{(Q)} := \hat{M}_{\gamma} \varepsilon_{\gamma\mu\nu} \varepsilon_{ik\ell} \, \partial_k Q_{\mu\alpha} \partial_\ell Q_{\nu\alpha} \,. \tag{2.15}$$

The tensor field \mathbf{D} , written in terms of either $\hat{\mathbf{n}}$ or \mathbf{Q} , thus contains spatial information about disclinations. Its definition here coincides with eqn (9) of Ref. [20], in which the properties of \mathbf{D} were explored for various disclination configurations. We note that the definition of $\mathbf{D}^{(\hat{\mathbf{n}})}$ is written to include both the second and third terms on the right-hand side of equation (2.11), so that $\mathbf{D}^{(\hat{\mathbf{n}})}$ may be used for both point defects and Skyrmions, as explored in §4.

It is important to point out that the first term on the right-hand side of equations (2.11) and (2.12), while zero at disclination cores, is not zero in general. As a consequence, a non-zero density \mathbf{D} could point to a spurious topological singularity where there is none. Away from defects, where it is possible $\hat{\mathbf{M}} \neq \hat{\mathbf{\Omega}}$, this term may be non-zero. This is the case, for example, in double-splay or double-twist configurations [33,34]. Since a double-splay or double-twist configuration is not a disclination, the integral in equation (2.9) must give zero, and so this term must also integrate to zero. That \mathbf{D} itself is non-zero for these special configurations (and perhaps others) is an interesting result, and more work is needed to fully understand it. It is likely due to the fact that \mathbf{D} is related to the Jacobian of the transformation between areas in configuration space and areas in subspaces of order parameter space. Real space patches of double-splay and double-twist configurations, for example, can be mapped to patches on the unit sphere. In §4, we explore some of the properties of \mathbf{D} for nematic configurations containing double-splay or double-twist.

3. Properties of **D** at disclinations

For completeness, and to give context for the results presented in §4, we briefly review some of the properties of \mathbf{D} for a disclination core [20]. For a disclination core located along a curve $\mathbf{R}(s)$, we assume the director near the core is given by equation (2.10). Substituting equation (2.10) into (2.14) gives

$$\mathbf{D}^{(\hat{\mathbf{n}})}(\mathbf{r}) = \pi \delta[\mathbf{r} - \mathbf{R}] (\hat{\boldsymbol{\Omega}} \otimes \hat{\mathbf{T}}), \tag{3.1}$$

so that $\mathbf{D}^{(\hat{\mathbf{n}})}$ is zero everywhere except the disclination core. On the other hand, if equation (2.13) is inserted into equation (2.15), we may approximate \mathbf{D} near the core as

$$\mathbf{D}^{(\mathbf{Q})}(\mathbf{r} \to \mathbf{R}) \approx \frac{s_N^2}{2a^2} (\hat{\boldsymbol{\Omega}} \otimes \hat{\mathbf{T}}). \tag{3.2}$$

Near the core where equation (2.13) holds, $|\mathbf{D}^{(Q)}|$ is constant; however, as one moves further from the core, the linear approximation fails to hold and instead \mathbf{Q} smoothly interpolates the core region to the constant $S = S_N$ region [19,24]. In this latter region, $\mathbf{D} = 0$ and so $|\mathbf{D}^{(Q)}(\rho)|$, where ρ is the radial cylindrical coordinate, smoothly goes from the constant given in equation (3.2) to zero. We show this for an equilibrium disclination line configuration in figure 2. The disclination line configuration was computed using the finite element Matlab/C++ package FELICITY and a gradient descent algorithm to minimize the free energy [3,35].

Equations (3.1) and (3.2) show that the tensor \mathbf{D} yields both the location and the geometric character of the disclination line from either $\hat{\mathbf{n}}$ or the tensor \mathbf{Q} . This result is useful for both experiments and numerical computation to conveniently locate a disclination line and to determine its local geometric character. One may extract $\hat{\boldsymbol{\Omega}}$ and $\hat{\mathbf{T}}$ from \mathbf{D} by computing the non-degenerate eigenvectors of $\mathbf{D}\mathbf{D}^T$ and $\mathbf{D}^T\mathbf{D}$, which give $\hat{\boldsymbol{\Omega}}$ and $\hat{\mathbf{T}}$, respectively [20].

4. Properties of **D** for configurations not involving disclinations

(a) Point defects

In three-dimensional nematics, point defects are also topologically allowed. These objects manifest as point singularities in the director field, and, like disclinations, feature long-ranged distortions of the nematic. The charge of a point defect may be measured by a surface integral:

$$m = \frac{1}{8\pi} \oint_{\partial \Omega} \hat{n}_{\nu} \left(\varepsilon_{\nu\mu\nu} \varepsilon_{ik\ell} \partial_{k} \hat{n}_{\mu} \partial_{\ell} \hat{n}_{\nu} \right) d\Sigma_{\nu}$$
(4.1)

where the surface of integration $\partial\Omega$ is a closed surface, and hence a boundary of a volume Ω . The term in the parentheses is precisely $\mathbf{D}^{(\hat{\mathbf{n}})}$, defined in equation (2.14), and thus we may write the charge as

$$m = \frac{1}{8\pi} \oint_{\partial\Omega} \hat{n}_{\gamma} D_{\gamma i}^{(\hat{\mathbf{n}})} d\Sigma_{i}. \tag{4.2}$$

Similar to the construction of the charge for a disclination line, we may generalize equation (4.2) to use the **Q**-tensor instead of $\hat{\mathbf{n}}$, resulting in

$$m = \frac{1}{8\pi S_N^2} \oint_{\partial \Omega^*} \hat{n}_{\gamma} D_{\gamma i}^{(\mathbf{Q})} d\Sigma_{i\nu}$$
 (4.3)

where $\partial\Omega^*$ denotes a surface such that the scalar order parameter remains constant, $S = S_N$. The integrands of equations (4.1) and (4.2) are similar to the quantity used to identify disclinations, equations (2.14) and (2.15), except that $\hat{\mathbf{n}}$ is projected into \mathbf{D} instead of $\hat{\mathbf{M}}$. Thus, we expect $\mathbf{D}^{(\hat{\mathbf{n}})}$ and $\mathbf{D}^{(\mathbf{Q})}$ to be useful in identifying point defects as well.

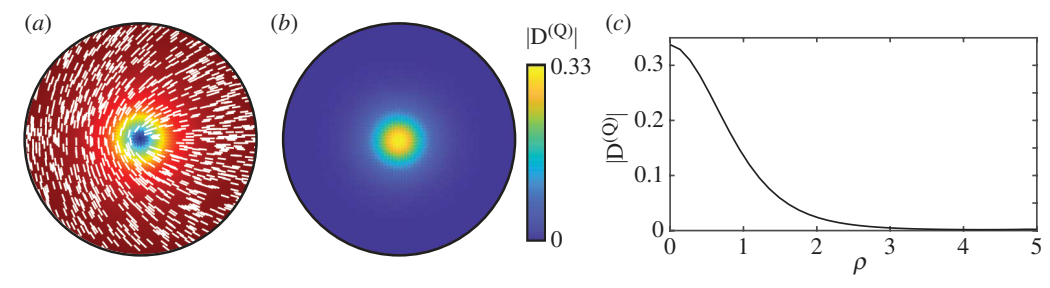


Figure 2. (a) Nematic profile of a cut through the normal plane of a wedge disclination, numerically computed using a \mathbf{Q} -tensor representation. The colour indicates the scalar order parameter, S. The white lines show the local director $\hat{\mathbf{n}}$. (b) Numerically computed spatial profile of $|\mathbf{D}^{(\mathbf{Q})}|$ for the disclination. (c) Plot of $|\mathbf{D}^{(\mathbf{Q})}(\rho)|$ extracted from (b).

The properties of $\mathbf{D}^{(\hat{\mathbf{n}})}$ and $\mathbf{D}^{(Q)}$ for point defects are different because of the director singularity. As an example, we compute $\mathbf{D}^{(\hat{\mathbf{n}})}$ explicitly for an ideal 'radial hedgehog' point defect with $\hat{\mathbf{n}} = \hat{\mathbf{r}}$:

$$\mathbf{D}^{(\hat{\mathbf{n}})} = \frac{2}{r^2} (\hat{\mathbf{r}} \otimes \hat{\mathbf{r}}) = \frac{2}{r^2} (\hat{\mathbf{n}} \otimes \hat{\mathbf{r}}), \tag{4.4}$$

where the second equality is written as a conjecture for a more general decomposition of $\mathbf{D}^{(\hat{\mathbf{n}})}$ for a point defect. Equation (4.4) shows that the tensor $\mathbf{D}^{(\hat{\mathbf{n}})}$ diverges at r=0, where the director singularity occurs. More interestingly, while $|\mathbf{D}^{(\hat{\mathbf{n}})}|$ decays rapidly, it does not go to zero at some finite distance. A plot of $|\mathbf{D}^{(\hat{\mathbf{n}})}(r)|$ is given in figure 3d. This behaviour is strikingly different than in the case of a disclination, in which $|\mathbf{D}^{(\hat{\mathbf{n}})}| \propto \delta(\mathbf{r})$ [equation (3.1)].

Downloaded from https://royalsocietypublishing.org/ on 16 September 2024

The decomposition of $\mathbf{D}^{(\hat{\mathbf{n}})}$ for disclinations into tangent and rotation vectors does not hold for point defects, as can be seen by comparing equations (3.1) and (4.4). We further probe the suggested decomposition in equation (4.4) by computing $\mathbf{D}^{(\hat{\mathbf{n}})}$ for a negative hedgehog point defect in which $\hat{\mathbf{n}} = -\cos 2\theta \hat{\mathbf{r}} + \sin 2\theta \hat{\boldsymbol{\theta}}$. In this case,

$$\mathbf{D}^{(\hat{\mathbf{n}})} = \frac{2}{r^2} \left[\cos 2\theta (\hat{\mathbf{r}} \otimes \hat{\mathbf{r}}) - \sin 2\theta (\hat{\boldsymbol{\theta}} \otimes \hat{\mathbf{r}}) \right] = -\frac{2}{r^2} (\hat{\mathbf{n}} \otimes \hat{\mathbf{r}}), \tag{4.5}$$

hence the charge of the defect is reflected in the sign of $\mathbf{D}^{(\hat{\mathbf{n}})}$, and the conjectured decomposition holds. We note that we have used here the convention that a positive hedgehog is one such that $\hat{\mathbf{n}} = +\hat{\mathbf{r}}$ pointing outward. However, the sign of $\mathbf{D}^{(\hat{\mathbf{n}})}$ changes if $\hat{\mathbf{n}} \to -\hat{\mathbf{n}}$ and so too will the measured charge, as reflected by equation (4.1). This 'local-to-global' problem is discussed in more detail in Ref. [23].

If we instead compute $\mathbf{D}^{(\mathbf{Q})}$ for a point defect, there is no longer a divergence at the defect core. This is because $\mathbf{Q} \to 0$ at the defect core to alleviate the diverging elastic energy, as shown in figure 3a, in which we have numerically computed the structure of a radial hedgehog defect by using the finite element Matlab/C++ package FELICITY to minimize a free energy in terms of \mathbf{Q} [3,35]. However, asymptotically $\mathbf{Q} \sim r^2$ at the core of a point defect [36,37], and so $\mathbf{D}^{(\mathbf{Q})} \to 0$. Thus, apparently, the topological information is lost at the core of the point defect. We have computed $\mathbf{D}^{(\mathbf{Q})}$ from the hedgehog profile in figure 3a, which is shown in figure 3b,c. We find $|\mathbf{D}^{(\mathbf{Q})}| \sim r^2$ close to the defect core, while $|\mathbf{D}^{(\mathbf{Q})}| \sim 1/r^2$ far from the defect core, where S is constant, as shown in the inset of figure 3c. This behaviour is a major difference from the case of disclinations in which $\mathbf{D}^{(\mathbf{Q})}$ is finite within the core region, and largest at the disclination core (figure 2). This apparent loss of topological information may be explained by the fact that

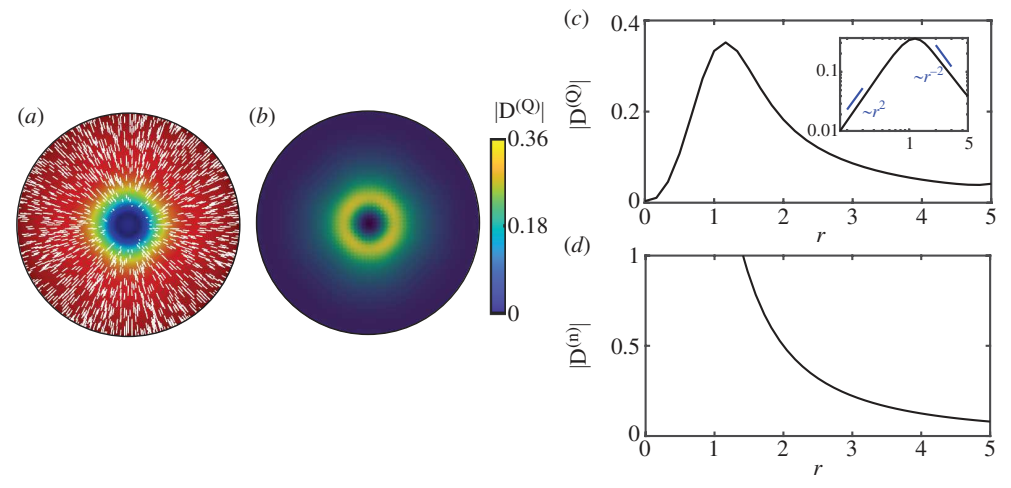


Figure 3. (a) Nematic profile of a cut through a radial hedgehog point defect, numerically computed using a \mathbf{Q} -tensor representation. The colour indicates the scalar order parameter, S, with $S \to 0$ at the defect core. The white lines show the local director $\hat{\mathbf{n}}$. (b) Numerically computed spatial profile of $|\mathbf{D}^{(\mathbf{Q})}|$ for the hedgehog point defect. (c) Plot of $|\mathbf{D}^{(\mathbf{Q})}(r)|$ extracted from (b). Inset: Same plot on logarithmic scaling axes. (d) Plot of $|\mathbf{D}^{(\hat{\mathbf{n}})}(r)|$, given by equation (4.4). Unlike $|\mathbf{D}^{(\mathbf{Q})}|$, $|\mathbf{D}^{(\hat{\mathbf{n}})}|$ diverges at the point defect core.

the full-order parameter space for **Q** is biaxial, and does not support point defects [38]. Hence, a point defect in the **Q**-tensor representation may dissociate into a biaxial disclination loop. Outside the core, when $S = S_N$ is constant, we still have $|\mathbf{D}^{(\mathbf{Q})}| \sim 1/r^2$ and so equation (4.3) still holds, since we only consider surfaces in which $S = S_N$ throughout the surface.

Finally, because the surface integrated over in equation (4.1) is closed, one may ask if a topological charge density akin to **D** for disclinations may be defined. Applying Gauss' law to equations (4.2) and (4.3) yields:

$$m = \frac{1}{8\pi} \int_{\Omega} \partial_i \left(\hat{n}_{\gamma} D_{\gamma i}^{(\hat{\mathbf{n}})} \right) dV, \tag{4.6}$$

$$m = \frac{1}{8\pi S_N^2} \int_{\Omega^*} \delta_i \left(\hat{n}_{\gamma} D_{\gamma i}^{(\mathbf{Q})} \right) dV . \tag{4.7}$$

The integrands of the above equations act as effective point defect densities. For the positive and negative hedgehogs computed above, the density is $\nabla \cdot \left(\hat{\mathbf{n}} \cdot \mathbf{D}^{(\hat{\mathbf{n}})} \right) \propto \delta(r)$ as expected. On the other hand, $\nabla \cdot \left(\hat{\mathbf{n}} \cdot \mathbf{D}^{(Q)} \right)$ is a diffuse scalar field that is still zero at the core of the point defect, but non-zero in the region surrounding the core in which \mathbf{Q} is varying.

(b) Double-splay and double-twist

The tensor **D** may also be non-zero in specific configurations that do not contain a topological defect, for example, in configurations with double-splay or double-twist distortion. We can explicitly calculate **D** in this case by considering $\hat{\bf n} = \cos k\rho \hat{\bf z} + \sin k\rho \hat{\bf \rho}$ in cylindrical coordinates. This is an ideal 'double-splay' configuration where the director is splayed in both directions, and k characterizes the inverse length scale of the distortion (see figure 4a for an example of double-splay in a splay-stabilized Skyrmion). A double-twist configuration can be obtained by replacing $\hat{\bf \rho} \to \hat{\bf \rho}$ in the equation for $\hat{\bf n}$. The tensor ${\bf D}^{(\hat{\bf n})}$ is:

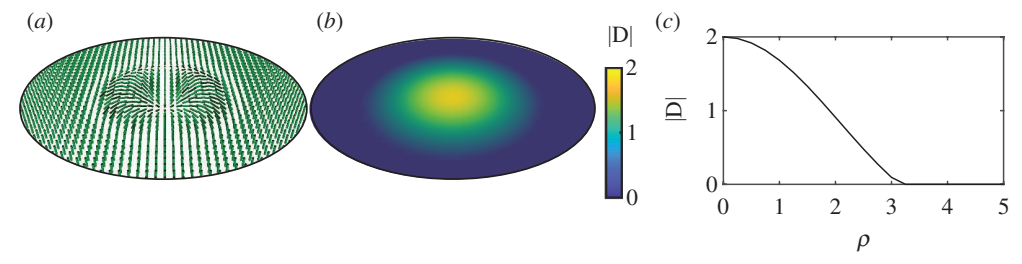


Figure 4. (*a*) Director field associated with a circular, splay-stabilized Skyrmion of radius π . (*b*) Spatial profile of $|\mathbf{D}|$ for the Skyrmion. (*c*) $|\mathbf{D}(\rho)|$ given by equation (4.13).

$$\mathbf{D}^{(\hat{\mathbf{n}})} = \frac{2k\sin^2 k\rho}{\rho} (\hat{\boldsymbol{\rho}} \otimes \hat{\mathbf{z}}) + \frac{2k\cos k\rho \sin k\rho}{\rho} (\hat{\mathbf{z}} \otimes \hat{\mathbf{z}}). \tag{4.8}$$

Since the double-splay configuration is characterized only by a director deformation, $\mathbf{D}^{(\mathbf{Q})} = S_N^2 \mathbf{D}^{(\hat{\mathbf{n}})}$. This holds for any configuration in which $S = S_N$ is constant. Thus, for double-splay and double-twist distortions, $\mathbf{D} \neq 0$.

On the other hand, computing the charge defined in equation (2.9) by integrating along a curve around the double splay configuration will yield zero, since the curve does not encircle a disclination. We may show this explicitly by computing the loop integral for a circle of radius ρ with $k = \pi$. Using $\hat{\mathbf{n}}^* = \cos \pi \rho \hat{\mathbf{z}} + \sin \pi \rho \hat{\mathbf{x}}$, the charge integral is

$$-\tan \pi \rho \oint \frac{\sin \phi \, d\phi}{\sqrt{2 - 2\cos \phi + \sin^2 \phi \tan^2 \pi \rho}} = \begin{cases} 0 & \rho \neq \frac{1}{2} \\ -2\pi & \rho = \frac{1}{2} \end{cases}$$
(4.9)

which is always zero modulo 2π as expected. The charge defined in equation (2.9) along any curve C is zero in this configuration. This is because the corresponding curve in order parameter space will either not pass through the equator, or will do so an even number of times giving zero modulo two. As is well known, it is possible to continuously remove the distortion of this configuration to yield an undefected configuration.

Despite the existence of regular configurations with non-zero **D**, the tensor as defined is still useful to locate true singularities in both experiments and numerical computations since local relaxation can quickly remove large but regular distortions in systems in which the free energy penalizes them. Nevertheless, there are several liquid crystal systems that do support double-splay and double-twist distortions energetically. These are primarily cholesterics, in which the nematogens break chiral symmetry and in turn support spontaneous twist deformations [22]. These systems have been shown to exhibit spontaneous double-twist regions separated by disclinations, known as 'blue phases' [39,40]. Additionally, and more recently, lyotropic chromonic liquid crystals have been shown to exhibit spontaneous double-twist configurations in confinement [41–43]. Further, topological defects other than disclinations may exhibit regions of double-splay and double-twist. For example, in liquid crystals that have a strong response to external fields, topological defects known as 'Skyrmions' may form when an external field is introduced [27,31,34]. These defects are not disclinations, and instead share properties with Skyrmions in magnetic systems [44] and contain double-splay or double-twist configurations. We explicitly explore the properties of **D** for Skyrmions in the next section.

In systems in which elasticity or confinement promotes double-splay or double-twist configurations, one would need to consider the director $\hat{\mathbf{n}}$ or the tensor order parameter \mathbf{Q} in addition to \mathbf{D} to fully characterize regions where \mathbf{D} is non-zero. This is not a problem, however, since \mathbf{D} is computed from $\hat{\mathbf{n}}$ or \mathbf{Q} in the first place. Alternatively, formally, one may use the contour integral methodology as laid out above to unambiguously identify the existence of a disclination.

royalsocietypublishing.org/journal/rspa Proc. R. Soc. A 480: 20230564

(c) Skyrmions

Skyrmions are soliton-like topological defects that may occur in cholesterics or in liquid crystals with a strong response to external fields [27,31,34]. Unlike disclinations or hedgehogs, Skyrmions do not produce long-ranged distortions of the nematic, and, instead, the nematic distortion is limited to a finite area, as shown in figure 4a. Furthermore, the Skyrmion nematic texture is not associated with a singularity in $\hat{\bf n}$ and, thus, the tensor order parameter ${\bf Q}$ is not necessary to study the detailed structure of the defect. Despite these differences, the topological charge for a Skyrmion may still be defined via an integral similar to that for point defects,

$$m = \frac{1}{8\pi} \int_{\Gamma} \hat{n}_{\gamma} \left(\varepsilon_{\gamma\mu\nu} \varepsilon_{ik\ell} \partial_{k} \hat{n}_{\mu} \partial_{\ell} \hat{n}_{\nu} \right) d\Sigma_{i}. \tag{4.10}$$

Importantly, the surface Γ that is integrated over is not closed and must 'cover' the Skyrmion, otherwise a partial charge will be measured. As for point defects, the quantity in parentheses is precisely the tensor $\mathbf{D}^{(\hat{\mathbf{n}})}$, defined in equation (2.14), such that there is no singularity in the director field. We may then rewrite equation (4.10) as:

$$m = \frac{1}{8\pi} \int_{\Gamma} \hat{n}_{\gamma} D_{\gamma i}^{(\hat{\mathbf{n}})} d\Sigma_{i\gamma}$$
 (4.11)

$$m = \frac{1}{8\pi S_N^2} \int_{\Gamma} \hat{n}_{\gamma} D_{\gamma i}^{(\mathbf{Q})} d\Sigma_{ii}$$
 (4.12)

where the second equation is a generalization of the charge integral using the **Q**-tensor. Since there is no singularity, *S* should, in principle, be constant everywhere in the texture, so there is no difference in using the director representation versus the **Q** tensor representation (i.e. $\mathbf{D}^{(\mathbf{Q})} = S_N^2 \mathbf{D}^{(\hat{\mathbf{n}})}$).

As discussed above, for Skyrmions, $\mathbf{D}^{(\hat{\mathbf{n}})}$ will be non-zero due to the double-splay or double-twist configurations characteristic of these textures [34]; however, the decomposition into tangent and rotation vectors, equation (3.1), will not hold for this type of distortion. We may calculate $\mathbf{D}^{(\hat{\mathbf{n}})}$ for an idealized, circular, splay-stabilized Skyrmion in which the director is given by $\hat{\mathbf{n}} = \cos k\rho \hat{\mathbf{p}} + \sin k\rho \hat{\boldsymbol{\rho}}$ ($0 \le \rho \le \pi/k$). As in equation (4.8), we find

$$\mathbf{D}^{(\hat{\mathbf{n}})} = \frac{2k\sin^2 k\rho}{\rho} (\hat{\boldsymbol{\rho}} \otimes \hat{\mathbf{z}}) + \frac{2k\cos k\rho \sin k\rho}{\rho} (\hat{\mathbf{z}} \otimes \hat{\mathbf{z}}) = \frac{2k\sin k\rho}{\rho} (\hat{\mathbf{n}} \otimes \hat{\mathbf{z}})$$
(4.13)

for $0 \le \rho \le \pi/k$ and $\mathbf{D}^{(\hat{\mathbf{n}})} = 0$ for $\rho > \pi/k$. In this case, $\mathbf{D}^{(\hat{\mathbf{n}})}$ has a diffuse, non-zero magnitude regardless of the representation of nematic. $|\mathbf{D}|$ is shown in figure 4b,c for an ideal, splay-stabilized Skyrmion. Furthermore, while the decomposition equation (3.1) does not hold, $\mathbf{D}^{(\hat{\mathbf{n}})} \propto (\hat{\mathbf{n}} \otimes \hat{\mathbf{N}})$, where $\hat{\mathbf{N}}$ is the normal vector to the plane of the Skyrmion distortion. We note that the structure of \mathbf{D} for Skyrmions differs significantly from that of both disclinations and point defects. This difference should allow one to use \mathbf{D} to distinctly characterize the unique topological structures that exist in nematics.

5. Conclusions

We have introduced an exact expression defining the topological charge of line defects encircled by an arbitrary path in \mathbb{RP}^2 . It yields π for configurations with net disclination charge and zero otherwise, as required by the topology of disclinations in three-dimensional nematics. This method may be used to unambiguously identify disclinations given any path in order parameter space.

royalsocietypublishing.org/journal/rspa Proc. R. Soc. A 480: 20230564

While the path integral expression for topological charge introduced here is an important mathematical result and should be a useful tool for method verification in experimental and computational studies, it may not be as practically useful as other current methods employed in large-scale studies due to the complicated nature of the construction. Fortunately, as we have shown, the integral over paths can be conveniently transformed into surface integrals involving the tensor density **D**. While **D** is a useful quantity to identify and locate disclination lines from both the director and tensor order parameter fields, it can also be non-zero in certain configurations that do not contain disclinations. For example, double-splay and double-twist nematic configurations generically yield a non-zero **D**, which results in a non-zero **D** for other topologically protected objects such as Skyrmions and point defects. For these objects, we have shown that **D** has different properties than for the case of disclinations, but that it may still be used to identify and potentially characterize them.

Elucidating the consequences of topological constraints on the properties and evolution of non-equilibrium soft matter systems remains a very active area of research. Our results provide the tools to diagnose the existence of disclination lines in experimentally determined or computationally generated configurations of nematics, as well as predicting and tracking their motion. Further research is needed to confirm the decomposition of **D** proposed for both Skyrmions and point defects as our results apply to specific, idealized, configurations, but we have not proven them for general cases. Additionally, we have focused here on **D** as defined for nematic phases but it appears possible that a similar tensor may be defined for other systems such as smectics or magnetic materials. It is already known that a similar object exists for dislocations in solids [45,46]. Finally, as demonstrated in Ref. [21], there is a direct connection between **D** and disclination dynamics. It remains to be examined whether a similar connection could be made to understand the dynamics of Skyrmions and point defects.

Data accessibility. This article has no additional data.

Declaration of Al use. We have not used AI-assisted technologies in creating this article.

Authors' contributions. C.D.S.: conceptualization, formal analysis, methodology, writing—original draft; J.V.: methodology, validation, writing—review and editing.

Both authors gave final approval for publication and agreed to be held accountable for the work performed therein.

Conflict of interest declaration. We declare we have no competing interests.

Funding. This research has been supported by the National Science Foundation under Grant Nos. DMR-1838977 and DMR-2223707, and by the Minnesota Supercomputing Institute. C.D.S. acknowledges support from the U.S. Department of Energy through the Los Alamos National Laboratory. Los Alamos National Laboratory is operated by Triad National Security, LLC, for the National Nuclear Security Administration of U.S. Department of Energy (Contract No. 89233218CNA000001).

Acknowledgements. We are indebted to Jonathan Selinger for clarifying the scope of the definition of the tensor D. His comments led to the redefinition of its path integral around a disclination core from the earlier version given in [20].

Appendix A. Distance between points in Euclidean space

The idea behind the invariant integral, equation (2.8), is that it gives the geodesic distance between two points on the hemisphere, and hence it can only be zero or π for closed curves. We prove that this is the case in equations (2.6) and (2.7). To provide extra clarity and context to that result, we show here how a similar construction may be made in Euclidean space.

We first write the definition for the arclength of an arbitrary curve in the following way:

$$A = \int_{C} \left(\hat{\mathbf{T}}(s) \cdot \hat{\mathbf{T}}(s) \right) ds, \tag{A 1}$$

where $\hat{\mathbf{T}}(s)$ is the tangent vector to the curve C, parameterized by $\gamma(s)$, with s an arclength parameter. This form of the arclength is similar to the form we have for the arclength of a curve

royalsocietypublishing.org/journal/rspa Proc. R. Soc. A **480:** 20230564

on the sphere in terms of $\hat{\bf n}$. To make an analogy with the construction in the main text, we define

$$\mathbf{\hat{T}}^*(s) = \frac{\gamma(s) - \gamma(0)}{|\gamma(s) - \gamma(0)|}.$$
 (A 2)

This is the tangent vector of the straight line segment starting from $\gamma(0)$ and ending at $\gamma(s)$, and so is the equivalent of $\hat{\mathbf{T}}_{GC}$ in equation (2.1).

Now, instead of the arclength, we compute the integral $\mathcal{L}(\hat{\mathbf{T}}^* \cdot \hat{\mathbf{T}})$ ds. This is equivalent to the integral (2.6). We compute

$$\int_0^A \left(\mathbf{\hat{T}}^* \cdot \mathbf{\hat{T}} \right) ds = \int_0^A \frac{\gamma(s) - \gamma(0)}{|\gamma(s) - \gamma(0)|} \cdot \frac{d\gamma}{ds} ds = \int_0^A \frac{d}{ds} (|\gamma(s) - \gamma(0)|) ds = |\gamma(A) - \gamma(0)|. \tag{A 3}$$

The final result is just the distance between the two endpoints of the curve, rather than the arclength of the curve.

References

- 1. Schimming CD, Viñals J. 2020 Anisotropic disclination cores in nematic liquid crystals modeled by a self-consistent molecular field theory. *Phys. Rev. E* **102**, 010701. (doi:10.1103/PhysRevE.102.010701)
- Guo Y, Jiang M, Afghah S, Peng C, Selinger RLB, Lavrentovich OD, Wei QH. 2021 Photopatterned designer disclination networks in nematic liquid crystals. *Adv. Opt. Mater.* 9, 2100181. (doi:10.1002/adom.202100181)
- 3. Schimming CD, Viñals J, Walker SW. 2021 Numerical method for the equilibrium configurations of a Maier-Saupe bulk potential in a Q-tensor model of an anisotropic nematic liquid crystal. *J. Comput. Phys.* **441**, 110441. (doi:10.1016/j.jcp.2021.110441)
- Zushi Y, Takeuchi KA. 2022 Scaling and spontaneous symmetry restoring of topological defect dynamics in liquid crystal. *Proc. Natl Acad. Sci. USA* 119, e2207349119. (doi:10.1073/ pnas.2207349119)
- 5. Wang M, Li Y, Yokoyama H. 2017 Artificial web of disclination lines in nematic liquid crystals. *Nat. Commun.* **8**, 388. (doi:10.1038/s41467-017-00548-x)
- Modin A, Ash B, Ishimoto K, Leheny RL, Serra F, Aharoni H. 2023 Tunable threedimensional architecture of nematic disclination lines. *Proc. Natl Acad. Sci. USA* 120, e2300833120. (doi:10.1073/pnas.2300833120)
- Ravnik M, Skarabot M, Zumer S, Tkalec U, Poberaj I, Babic D, Osterman N, Musevic I. 2007 Entangled nematic colloidal dimers and wires. *Phys. Rev. Lett.* 99, 247801. (doi:10.1103/ PhysRevLett.99.247801)
- Copar S, Zumer S. 2011 Nematic braids: topological invariants and rewiring of disclinations. Phys. Rev. Lett. 106, 177801. (doi:10.1103/PhysRevLett.106.177801)
- 9. Peng C, Guo Y, Conklin C, Viñals J, Shiyanovskii SV, Wei QH, Lavrentovich OD. 2015 Liquid crystals with patterned molecular orientation as an electrolytic active medium. *Phys. Rev. E* **92**, 052502. (doi:10.1103/PhysRevE.92.052502)
- Conklin C, Viñals J. 2017 Electrokinetic flows in liquid crystal thin films with fixed anchoring. Soft Matter 13, 725–739. (doi:10.1039/c6sm02393b)
- 11. Saw TB *et al.* 2017 Topological defects in epithelia govern cell death and extrusion. *Nature* 544, 212–216. (doi:10.1038/nature21718)
- 12. Opathalage A, Norton MM, Juniper MPN, Langeslay B, Aghvami SA, Fraden S, Dogic Z. 2019 Self-organized dynamics and the transition to turbulence of confined active nematics. *Proc. Natl Acad. Sci. USA* **116**, 4788–4797. (doi:10.1073/pnas.1816733116)
- 13. Duclos G et al. 2020 Topological structure and dynamics of three-dimensional active nematics. *Science* **367**, 1120–1124. (doi:10.1126/science.aaz4547)

- 15. Zhang R *et al.* 2021 Spatiotemporal control of liquid crystal structure and dynamics through activity patterning. *Nat. Mater.* **20**, 875–882. (doi:10.1038/s41563-020-00901-4)
- 16. Meng C, Wu JS, Smalyukh II. 2023 Topological steering of light by nematic vortices and analogy to cosmic strings. *Nat. Mater.* 22, 64–72. (doi:10.1038/s41563-022-01414-y)
- 17. Tang X, Selinger JV. 2017 Orientation of topological defects in 2D nematic liquid crystals. *Soft Matter* **13**, 5481–5490. (doi:10.1039/c7sm01195d)
- 18. Angheluta L, Chen Z, Marchetti MC, Bowick MJ. 2021 The role of fluid flow in the dynamics of active nematic defects. *New J. Phys.* 23, 033009. (doi:10.1088/1367-2630/abe8a8)
- 19. Long C, Tang X, Selinger RLB, Selinger JV. 2021 Geometry and mechanics of disclination lines in 3D nematic liquid crystals. *Soft Matter* 172265–2278, (doi:10.1039/d0sm01899f)
- Schimming CD, Viñals J. 2022 Singularity identification for the characterization of topology, geometry, and motion of nematic disclination lines. Soft Matter 18, 2234–2244. (doi:10.1039/ d1sm01584b)
- 21. Schimming CD, Viñals J. 2023 Kinematics and dynamics of disclination lines in three-dimensional nematics. *Proc. R. Soc. A* **479**, 20230042. (doi:10.1098/rspa.2023.0042)
- 22. de Gennes PG, Alben R. 1975 The physics of liquid crystals. *Phys. Today* **28**, 54–55. (doi:10. 1063/1.3069010)
- Alexander GP, Chen B ge, Matsumoto EA, Kamien RD. 2012 Colloquium: disclination loops, point defects, and all that in nematic liquid crystals. Rev. Mod. Phys. 84, 497–514. (doi:10. 1103/RevModPhys.84.497)
- Schopohl N, Sluckin T. 1987 Defect core structure in nematic liquid crystals. *Phys. Rev. Lett.* 59, 2582–2584. (doi:10.1103/PhysRevLett.59.2582)
- 25. Stark H. 2001 Physics of colloidal dispersions in nematic liquid crystals. *Phys. Rep.* **351**, 387–474. (doi:10.1016/S0370-1573(00)00144-7)
- Lazo I, Peng C, Xiang J, Shiyanovskii SV, Lavrentovich OD. 2014 Liquid crystal-enabled electro-osmosis through spatial charge separation in distorted regions as a novel mechanism of electrokinetics. *Nat. Commun.* 5, 5033. (doi:10.1038/ncomms6033)

Downloaded from https://royalsocietypublishing.org/ on 16 September 2024

- 27. Ackerman PJ, Trivedi RP, Senyuk B, van de Lagemaat J, Smalyukh II. 2014 Two-dimensional skyrmions and other solitonic structures in confinement-frustrated chiral nematics. *Phys. Rev. E* **90**, 012505. (doi:10.1103/PhysRevE.90.012505)
- Li X et al. 2017 Directed Self-assembly of colloidal particles onto nematic liquid crystalline defects engineered by chemically patterned surfaces. ACS Nano 11, 6492–6501. (doi:10.1021/ acsnano.7b03641)
- 29. Peng C, Turiv T, Guo Y, Wei QH, Lavrentovich OD. 2018 Sorting and separation of microparticles by surface properties using liquid crystal-enabled electro-osmosis. *Liq. Cryst.* **45**, 1936–1943. (doi:10.1080/02678292.2018.1481539)
- 30. Duzgun A, Nisoli C. 2021 Skyrmion spin ice in liquid crystals. *Phys. Rev. Lett.* **126**, 047801. (doi:10.1103/PhysRevLett.126.047801)
- 31. Duzgun A, Nisoli C, O Reichhardt CJ, Reichhardt C. 2022 Directed motion of liquid crystal skyrmions with oscillating fields. *New J. Phys.* **24**, 033033. (doi:10.1088/1367-2630/ac58b8)
- 32. Efrati E, Irvine WTM. 2014 Orientation-dependent handedness and chiral design. *Phys. Rev. X* **4**, 011003. (doi:10.1103/PhysRevX.4.011003)
- 33. Selinger JV. 2018 Interpretation of saddle-splay and the Oseen-Frank free energy in liquid crystals. *Liq. Cryst. Rev.* **6**, 129–142. (doi:10.1080/21680396.2019.1581103)
- 34. Long C, Selinger JV. 2021 Coarse-grained theory for motion of solitons and skyrmions in liquid crystals. *Soft Matter* **17**, 10437–10446. (doi:10.1039/d1sm01335a)
- Walker SW. 2018 FELICITY: A Matlab/C++ Toolbox for Developing Finite Element Methods and Simulation Modeling. SIAM J. Sci. Comput. 40, C234–C257. (doi:10.1137/17M1128745)
- Greco F, Marrucci G. 1992 Molecular structure of the hedgehog point defect in nematics. Mol. Cryst. Liq. Cryst. Sci. Technol. Sect. A Mol. Cryst. Liq. Cryst. 210, 129–141. (doi:10.1080/10587259208030761)
- 37. Majumdar A. 2012 The radial-hedgehog solution in Landau–de Gennes' theory for nematic liquid crystals. *Eur. J. Appl. Math.* 23, 61–97. (doi:10.1017/S0956792511000295)

- 38. Pismen LM. 1999 Vortices in Nonlinear fields. In *Vortices in Nonlinear fields: from liquid crystals to Superfluids, from non-equilibrium patterns to cosmic strings*. New York, NY: Oxford University Press. (doi:10.1093/oso/9780198501671.001.0001)
- 39. Meiboom S, Sammon M, Brinkman WF. 1983 Lattice of disclinations: the structure of the blue phases of cholesteric liquid crystals. *Phys. Rev. A* 27, 438–454. (doi:10.1103/PhysRevA. 27.438)
- 40. Wright DC, Mermin ND. 1989 Crystalline liquids: the blue phases. *Rev. Mod. Phys.* **61**, 385–432. (doi:10.1103/RevModPhys.61.385)
- 41. Tortora L, Lavrentovich OD. 2011 Chiral symmetry breaking by spatial confinement in tactoidal droplets of lyotropic chromonic liquid crystals. *Proc. Natl Acad. Sci. USA* **108**, 5163–5168. (doi:10.1073/pnas.1100087108)
- Davidson ZS, Kang L, Jeong J, Still T, Collings PJ, Lubensky TC, Yodh AG. 2015 Chiral structures and defects of lyotropic chromonic liquid crystals induced by saddle-splay elasticity. *Phys. Rev. E* 91, 050501. (doi:10.1103/PhysRevE.91.050501)
- 43. Selinger JV. 2022 Director deformations, geometric frustration, and modulated phases in liquid crystals. *Annu. Rev. Condens. Matter. Phys.* **13**, 49–71. (doi:10.1146/annurev-conmatphys-031620-105712)
- 44. Fert A, Reyren N, Cros V. 2017 Magnetic skyrmions: advances in physics and potential applications. *Nat. Rev. Mater.* **2**. (doi:10.1038/natrevmats.2017.31)
- 45. Kleman M, Friedel J. 2008 Disclinations, dislocations, and continuous defects: a reappraisal. *Rev. Mod. Phys.* **80**, 61–115. (doi:10.1103/RevModPhys.80.61)
- 46. Skogvoll V, Angheluta L, Skaugen A, Salvalaglio M, Viñals J. 2022 A phase field crystal theory of the kinematics of dislocation lines. *J. Mech. Phys. Solids* **166**, 104932. (doi:10.1016/j. jmps.2022.104932)